Exploring the Scientific Utility of Combined Spaceborne Lidar and Lightning Observations of Thunderstorms

Timothy J. Lang[1] and Sarah D. Bang[1]

[1] NASA Marshall Space Flight Center, Huntsville, Alabama

Corresponding author: Timothy Lang (timothy.j.lang@nasa.gov)

Key Points:

- Co-located spaceborne lightning and lidar observations of thunderstorms were combined in a pathfinder study.
- Thunderstorm cloud-top heights behaved reasonably with latitude, compared to radar echo-top climatologies.
- Comparison to lidar validated the excellent performance of the Lightning Imaging Sensor surface glint filter.

Abstract

Approximately eight months of co-located spaceborne lidar and lightning observations were analyzed in a pathfinder study to understand the advantages and challenges of using these combined observations to understand thunderstorms. Data from the Lightning Imaging Sensor (LIS) and the Cloud-Aerosol Transport System (CATS) lidar were used when they overlapped on the International Space Station during March-October 2017. Using simple matching criteria, 8246 LIS flashes occurred within 25 km of the CATS ground track. CATS cloud-top heights near these flashes showed similar behavior with latitude when compared to a spaceborne radar-based climatology, but the lidar cloud tops were approximately 2-km higher than 20-dBZ radar echo tops. CATS cloud phase near LIS flashes was consistent with ice or mixed-phase more than 90% of the time, showing the value of using lightning observations to validate lidar-based feature masks. In addition, correlations between a proxy for LIS flash rate and CATS ice water path, cloud optical depth, and cloud-top height were low (0.38-0.42) but positive and highly statistically significant ($> 99\%$), suggesting lidar retrievals of cloud properties can be meaningfully compared with lightning observations despite lidar's known inability to penetrate deeply into optically thick clouds like thunderstorms. Finally, CATS was used to help diagnose LIS false alarms due to surface-based glint. The false alarm rate was approximately 0.1%, which demonstrated the excellent performance of the surface glint filter in the LIS processing code. The results suggest that fruitful scientific insights can be expected from larger combined lidar/lightning datasets.

Plain Language Summary

Data from a laser-based instrument called a lidar (which can measure clouds and aerosols) and an optically based lightning detection instrument, both hosted on the International Space Station during March-October 2017, were used to study global thunderstorms from space. Because these types of instruments

have only been rarely combined in the past, this study focused on analyzing a small dataset in order to determine how useful the instrument combination can be. The results found that thunderstorm cloud-top heights slope downward from the Equator toward the poles, similar to how the tropopause height also slopes downward. Lidar measurements of cloud properties, like cloud-top height and the amount of ice in the cloud, were quantitatively related to lightning observations like flash rate. The lidar also was helpful in finding instances where the lightning instrument accidentally detected glint from the sun on water, snow, etc. instead of lightning, because there were no lidar-detected clouds nearby. However, this rarely occurred due to how the lightning instrument's data are processed. Additional fruitful scientific insights can be expected from other, larger combined lidar/lightning datasets.

1 Introduction

1.1 Background

Lidar is a common tool for measuring clouds, aerosols, and atmospheric state, and has been used for many decades from ground-based (e.g., Sassen, 1977), airborne (e.g., McGill et al., 2007), and spaceborne platforms (e.g., Winker et al., 2006). A fundamental aspect of lidar is its difficulty in penetrating deeply into optically thick clouds, such as cumulonimbus (i.e., thunderstorms). Nevertheless, some studies have successfully used lidar to study characteristics of deep convection, thunderstorms, and even lightning. For example, Sassen (1977) took advantage of relatively high-altitude cloud bases in Wyoming to use a ground-based lidar to study the optical scattering characteristics of melting precipitation in summertime thunderstorms. Airborne lidars have been used to document many aspects of thunderstorms as well as their surrounding environments. For example, Sassen et al. (2000) and Campbell et al. (2005) used lidar to study the microphysical properties of deep convective cloud tops and thunderstorm anvils. These studies often have made use of polarization-diversity lidar measurements to infer cloud-particle phase, habit, and orientation within these anvils, qualitatively similar to how polarimetric microwave radar has been used to study precipitation characteristics deep within thunderstorms (e.g., Kumjian & Ryzhkov, 2008). Outside of precipitation, airborne lidar has been used to quantify wind profiles near deep convection (e.g., Cui et al., 2020). Meanwhile, ground-based ozone lidars have been used to document lightning-produced nitrogen oxides (NOx) in the vicinity of thunderstorms (Wang et al., 2015). Lidar has even been proposed as a method to remotely sense electromagnetic fields in order to estimate the possibility of lightning strikes outside of clouds (Shiina et al., 2006).

Combined observations of deep convection from radar, microwave radiometers, infrared spectrometers, and lidar have also been made (Heymsfield & Fulton, 1988; McGill et al., 2004; van Diedenhoven et al., 2016). Indeed, these combined measurements with lidar and other instruments form the scientific basis for the CloudSat and Cloud-Aerosol Lidar and Infrared Pathfinder Satellite Observation (CALIPSO) missions (Mace et al., 2009), as well as the overall A-Train

satellite constellation (Delanoe & Hogan, 2010) and the future Atmosphere Observing System (AOS, 2022). Such combined measurements can enable more accurate retrievals of microphysical processes near cloud top.

However, detailed comparisons between lightning and lidar observations are rare in the literature. One notable recent study was Allen et al. (2021), which made use of airborne observations from the Fly's Eye Geostationary Lightning Mapper Simulator (FEGS; Quick et al., 2021), the Cloud Physics Lidar (CPL; McGill et al., 2002), and an ultraviolet (UV) visible spectrometer to estimate NOx production by lightning. The role played by CPL was to measure cloud-top pressure, which played an important role in the NOx calculations, while FEGS was used to document the detection efficiencies of ground-based and spaceborne lightning observations for the storms that were studied. However, the airborne lidar and lightning observations were not directly compared to better resolve thunderstorm structure or processes. Moreover, coupled spaceborne lidar/lightning studies do not appear to exist in the literature. Potential advantages and challenges of doing more direct lidar/lightning comparisons are discussed below, particularly from the perspective of spaceborne platforms.

1.2 Potential advantages of using spaceborne lidar to study thunderstorms

Some potential advantages of spaceborne lidar include its ability to provide a more accurate measurement of cloud-top characteristics than, for example, spaceborne radar. Cloud-top height has previously been related to lightning flash rate (e.g., Price & Rind, 1992). In addition, lightning within the overshooting tops of thunderstorms has been shown to be of significance to thunderstorm electrification and charge structure (MacGorman et al., 2017). However, echo-top height as determined by radar strongly depends on the sensitivity of the radar itself. For example, the Ku-band radar used in the Tropical Rainfall Measuring Mission (TRMM), and the Ku- and Ka-band radars used in the Global Precipitation Measurement (GPM) mission, have minimum reflectivity sensitivities in excess of 10 dBZ (Kummerow et al., 1998; Hou et al., 2014). This means that these radars are not sensitive to the weaker echoes associated with true cloud tops (Hagihara et al., 2014). Lidar has been used to help diagnose cloud-top height underestimates in thermal imagery as well (e.g., Sherwood et al., 2004).

In addition, lidars are able to infer the dominant phase of hydrometeors near cloud top (Yoshida et al., 2010), as well as other microphysically related attributes like cloud optical depth and ice water content (IWC) and path (IWP; e.g., Avery et al., 2012). That being said, optical measurements do not penetrate deeply into thick clouds, particularly deep convection. However, studies like Rutledge et al. (2020) have demonstrated that near-cloud-top measurements of thunderstorms are useful as their optical properties have (among other things) implications for the detection efficiency of optically based lightning mappers like the Lightning Imaging Sensor (LIS; Kummerow et al., 1998; Blakeslee et al., 2020). In addition, lidars are capable of providing vertical structure information within the portions of clouds they do penetrate.

Lidars have been in space for longer than a decade (Winker, 2022), providing climate-quality records of cloud properties. This time period overlaps both LIS and Geostationary Lightning Mapper (GLM; Rudlosky et al. 2019) observations for many years. This means that there may be enough conjunctions between these two observations that useful analysis of thunderstorm properties could be performed. Moreover, lidars are planned to be part of the forthcoming AOS (2020), while GLMs and other spaceborne observations of lightning are also planned into the near future (e.g., Holmlund et al., 2021).

Though these data were not examined in this study, lidars are capable of detecting and categorizing aerosol properties (Ceolato & Berg, 2021). Since aerosols have been shown to be important for the strength and properties of convection, including thunderstorms (Khain et al., 2005), combining lidar observations of both cloud and aerosol properties with lightning observations could provide potentially useful information about thunderstorm-aerosol interactions. Moreover, it would be of interest to perform composition studies like Allen et al. (2021) using spaceborne platforms to provide a more global perspective on NOx production by lightning.

1.3 Potential challenges of using spaceborne lidar to study thunderstorms

All the above being said, there are significant challenges to using lidar to study thunderstorm properties. In addition to lidar's well-known inability to penetrate thick clouds, the sampling characteristics of spaceborne lidar and lightning observations are very different. For example, lightning observations from LIS and GLM are distributed horizontally, and include information about flash two-dimensional (2D) location (Rudlosky et al., 2019; Blakeslee et al., 2020). But they do not measure the vertical structure of lightning. On the other hand, lidars typically measure along a nadir curtain (Yorks et al., 2016; Winker, 2022), which means they provide vertically distributed observations that lack horizontal context. Thus, care needs to be taken when comparing spaceborne lidar and lightning datasets, but no well-tread analysis pathways exist with comparing these two datasets unlike, e.g., radar and lightning datasets (Rust & Doviak, 1982; Lopez & Aubagnac, 1997; Wiens et al., 2005; Carey et al., 2019). There is utility in exploring a small overlapping dataset of spaceborne lidar observations of thunderstorms, to better understand the advantages and challenges of doing this combined analysis, without committing significant resources on a "wild goose chase" if the analysis does not yield much scientific value.

1.4 Goals of this study

As it turns out, such a small overlapping dataset exists. For just short of 8 months in 2017, the Cloud-Aerosol Transport System (CATS) lidar (Yorks et al., 2016) overlapped with a LIS instrument on the International Space Station (ISS). As will be shown in this study, these co-located instruments provided a useful dataset for demonstrating the value of using lidar to study thunderstorm characteristics. This paper will discuss the advantages and challenges associated with this combined analysis, and will provide a path forward for more detailed

analysis using larger overlapping datasets.

2 Data and Methodology

2.1 ISS LIS

The International Space Station Lightning Imaging Sensor (ISS LIS) is a high-speed camera (500 frames per second) affixed to a telescope that detects lightning via monitoring transients at 777.4 nm. LIS is a modified flight spare of the TRMM LIS (1997-2015) instrument, hosted within the 5th Space Test Program – Houston (STP-H5) payload, launched in 2017.

ISS LIS extends TRMM LIS time series observations, expands latitudinal coverage, provides near-realtime data to operational users, and enables cross-sensor calibrations (e.g., with GLM). A thorough review of the ISS LIS sensor is provided in Blakeslee et al. (2020). The instrument's flash detection efficiency is approximately 60%, with sub-pixel (< 4 km) location accuracy and sub-frame (< 2 ms) timing accuracy. Quality-controlled, flash-level data and science backgrounds from ISS LIS (Blakeslee 2000a, b) were used in this study. These data are available starting 1 March 2017.

2.2 CATS

The CATS lidar made range-resolved measurements of clouds and aerosols at 1064 and 532 nm during 2015-2017 (Yorks et al., 2016). CATS had a vertical resolution of 60 m and a horizontal resolution of 5 km. The Level 2 products used in this study included vertical feature mask (e.g., liquid vs. frozen cloud, or aerosol type), as well as profiles of cloud properties (e.g., IWC, cloud optical depth).

CATS overlapped on the ISS with LIS during 1 March through 29 October 2017. After this period the CATS instrument's mission concluded. Coincidentally, the original CATS ray-tracing code was adapted and used within ISS LIS geolocation routines (Lang, 2019), which have been demonstrated to provide the aforementioned sub-pixel (< 4-km) location accuracy for LIS-detected lightning (Blakeslee et al., 2020). The previous TRMM-based LIS geolocation code was found to be not easily translated to the ISS.

2.3 Combining LIS with CATS

Combining the 2D horizontally distributed LIS dataset is not straightforward to do with the vertically profiling CATS lidar measurements. Since CATS provided a nadir-focused curtain, the first step to combining the datasets was to threshold on LIS flash centroid distance from the CATS ground track. During the nearly 8-month overlap period, this study determined that 8246 ISS LIS flashes had centroids within 25 km of the CATS ground track. The 25-km threshold was chosen to balance obtaining a co-location dataset large enough to enable useful statistical analysis, while still only comparing lightning that was close enough to the ground track to be potentially physically related to CATS-measured cloud properties. Sensitivity experiments were also performed with 50- and 10-km

ground-track distance thresholds. These results (not shown), were found to be qualitatively similar to the 25-km results discussed in this paper.

An example of a typical LIS/CATS matchup is shown in Fig. 1. Near 0903 UTC on 15 March 2017, CATS shows high-level cloud (close to 17 km MSL maximum height), a few km below which the signal is attenuated (Fig. 1a). The cloud itself is identified as primarily ice by the CATS feature mask (Fig. 1b). This is suggestive of the anvil region above and around deep convection. Meanwhile, more than a dozen ISS LIS flashes are identified whose centroids are within 25 km of the CATS ground track around this same time. This figure (and hundreds like it, not shown) demonstrate that these very different datasets can be combined to provide meaningful qualitative information about thunderstorms.

In order to explore the ability to retrieve more quantitative conclusions about thunderstorms using the combined dataset, an automated statistical analysis of CATS-retrieved cloud properties near ISS LIS measured lightning was performed. When lightning was observed, the maximum values of cloud parameters (e.g., IWP, cloud-top height, optical depth) within 50 km along the CATS track were determined. In addition, clusters of lightning flashes were identified (e.g., like in Fig. 1) using the Density-Based Spatial Clustering of Applications with Noise (DBSCAN) algorithm (Ester et al., 1996) with a minimum of 1 flash to create a cluster, and a maximum distance of 50 km between flashes in a cluster. The total number of flashes in each of these clusters was similarly compared to maximum values of CATS cloud properties within 50 km along the ground track. The use of the 50-km distance threshold along the track was to allow for the possibility that CATS did not gain a well-placed overpass of the relevant thunderstorm's core.

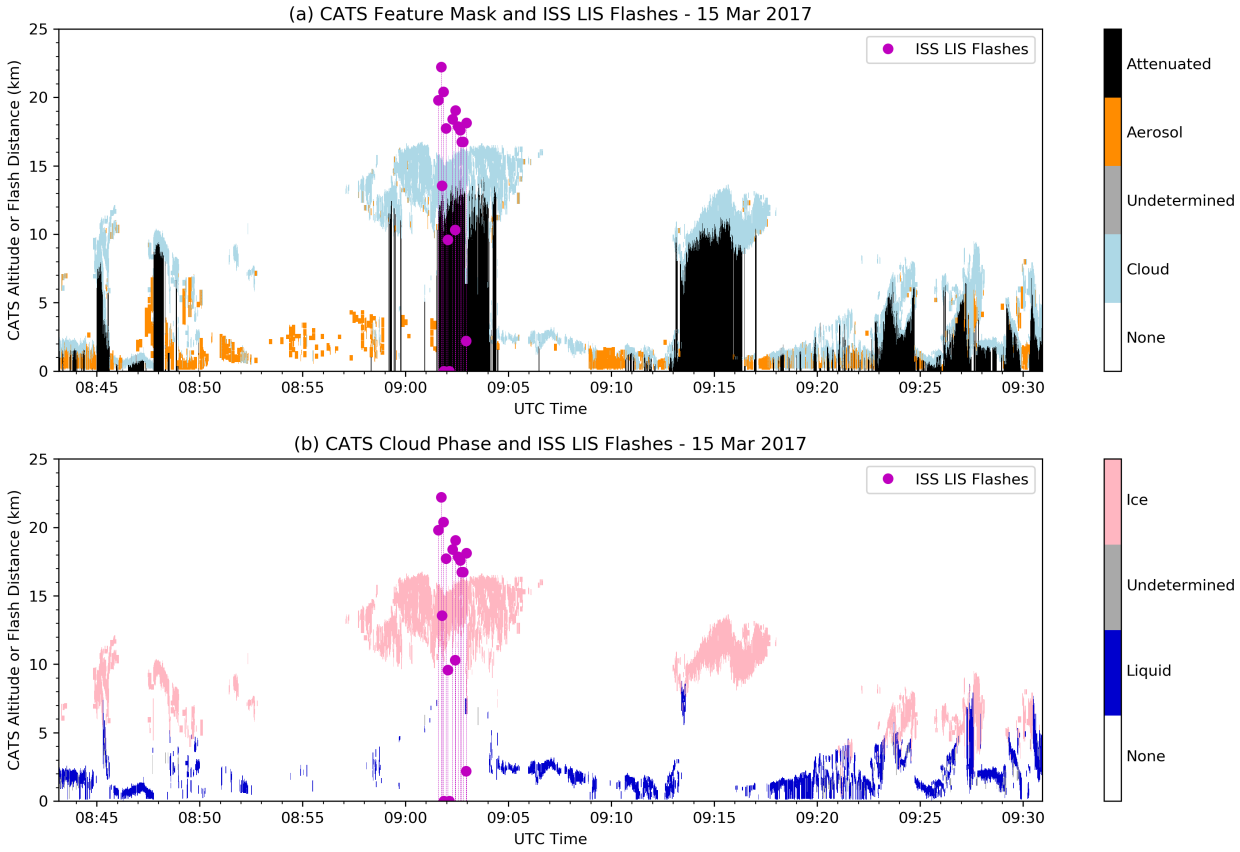

Figure 1. (a) Time-height plot of CATS feature mask with ISS LIS flashes overlaid for half an ISS orbit on 15 March 2017. ISS LIS flash times are plotted vs. distance from CATS ground track (not flash height, which LIS does not measure). (b) Time-height plot of CATS cloud phase with ISS LIS flashes overlaid for half an ISS orbit on 15 March 2017. ISS LIS flash times are plotted vs. distance from CATS ground track (not flash height, which LIS does not measure).

In addition to the above statistical analysis, a manual review of combined LIS/CATS quicklooks (e.g., Fig. 1) was performed. A major focus of this review was to identify LIS lightning that did not appear to occur near CATS-identified clouds. These potential false alarms were further studied using manual inspection of daytime LIS/CATS matchups using geolocated ISS LIS backgrounds, which are available every 30-60 seconds from LIS. These backgrounds (Blakeslee, 2020b) were geolocated using the *ISS_Camera_Geolocate* open-source software (Lang, 2019), originally developed in support of the Schultz et al. (2020) study.

2.4 Other datasets used

To assess the distribution of radar-observed echo-top heights, for comparison to CATS-measured thunderstorm cloud-top heights, we examine TRMM and Global Precipitation Measurement (GPM) Precipitation Features radar precipitation features (RPFs; Liu et al., 2008) for March through October 1998-2014 (TRMM) and 2014-2020 (GPM). The RPFs are defined as contiguous areas of at least 4 pixels of precipitation as detected by the TRMM Precipitation Radar (PR) or the GPM Dual-Frequency Precipitation Radar (DPR) Ku-band radars. These radars have minimum threshold reflectivities of 17 dBZ and 12 dBZ, respectively. Pixel size is roughly 20 km2. For each RPF, radar and passive microwave characteristics (e.g., echo-top heights, reflectivity profiles, and brightness temperatures) are provided, but in this study the focus was primarily on echo-top heights. In order define features with lightning, the coincident LIS data were used for TRMM RPFs. The GPM Core satellite does not have a lightning imager onboard, and therefore GPM RPFs were co-located with World Wide Lightning Location Network (WWLLN; Virts et al., 2013) data within a +/- 10-minute window in the boundary of the feature (Liu, 2020).

3 Results

3.1 Histograms of cloud- and echo-top height

Figure 2 shows a 2D histogram of CATS-measured maximum cloud-top-height vs. latitude within 50 km along the CATS ground track of at least one LIS-detected flash (Fig. 2a). The histogram is normalized but no adjustments for sampling frequency have been made due to the short time period of analysis (< 8 months). March-October 2017 primarily covers the spring, summer, and early fall seasons (i.e., warm season) in the northern hemisphere. Within 10° S to 20° N latitude, thunderstorm maximum cloud-top height was most frequently 16-17 km MSL. A downward sloping in maximum cloud-top height occurred toward the northern mid-latitudes, reflecting the general downward sloping of the tropopause toward the poles (Santer et al., 2003). Of course, as is well known thunderstorm heights are not fully constrained by the tropopause (Liu & Zipser, 2005). Regardless, within 35-50° N the thunderstorm cloud-top height most commonly ranged between 10 and 14 km MSL. Note the relatively few samples south of 10° S, reflecting the LIS/CATS dataset's focus on the northern hemisphere's warm season.

To help validate the conclusions implied by Fig. 2a, histograms for TRMM (Fig. 2b) and GPM RPF (Fig. 2c) maximum 20-dBZ echo-top height vs. latitude are shown for all RPFs with at least one LIS- or WWLLN-detected lightning flash during March through October (1998-2014 for TRMM, 2014-2020 for GPM). Due to the longer time periods for analysis, the TRMM and GPM histograms were normalized by sampling frequency. Note that TRMM was inclined at a much lower orbital angle (35°) than either ISS (57°) or GPM (65°), so latitudinal coverage was reduced relative to the other two platforms. Regardless, both TRMM and GPM suggest that thunderstorm 20-dBZ echo-top heights are lower by approximately 2 km than lidar-inferred cloud-top heights. The downward sloping of the echo-top heights toward the poles (with approximately the same

slope as Fig. 2a), as well as the preference for thunderstorms in the northern hemisphere during May-October, are also apparent. This suggests the added value of using a lidar over a radar to obtain a more accurate measurement of cloud-top height, but also implies a way to use lidar observations to help scale radar echo-top heights to cloud-top heights if only a radar is available (at least from an average global perspective). Moreover, this analysis also helps validate the matching criteria for the LIS/CATS comparison.

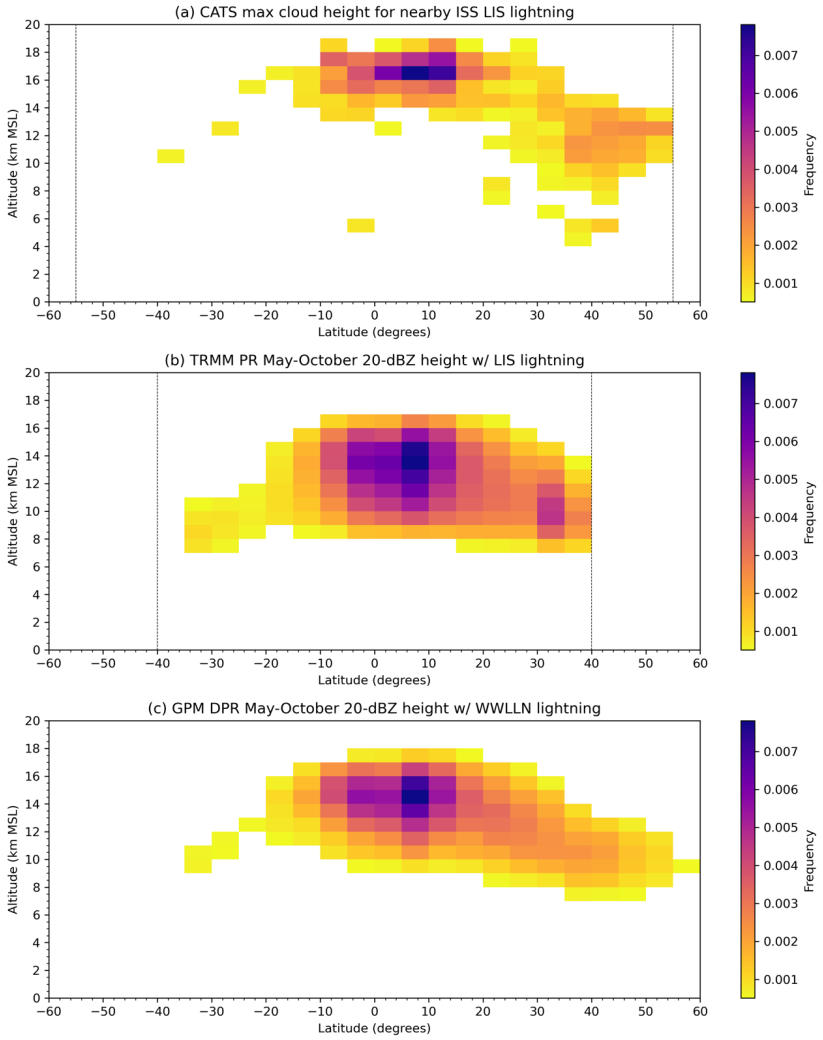

Figure 2. (a) Two-dimensional histogram of the frequency of CATS maximum cloud-top height vs. latitude, when at least one ISS LIS flash is detected, for March-October 2017. (b) Two-dimensional histogram of maximum 20-dBZ echo-top height vs. latitude for TRMM RPFs with at least one LIS-detected flash

during March-October 1998-2914. (c) Two-dimensional histogram maximum 20-dBZ echo-top height vs. latitude for GPM RPFs with at least one WWLLN-detected flash during March-October 2014-2020. Frequency values below 0.0005 are not shown in any of these subplots.

3.2 Comparison of thunderstorm characteristics

It is also of interest to compare LIS-detected lightning to CATS-inferred thunderstorm properties, such as IWP, dominant hydrometeor type, optical depth, and other characteristics. For this analysis, it is understood that a lidar cannot penetrate deeply into optically thick thunderstorms, and that statistical correlations thus will be significantly reduced compared to standard radar-lightning comparisons (Wiens et al., 2005; Carey et al., 2019). However, Rutledge et al. (2020) demonstrated that passive infrared measurements of cloud properties (again, largely limited to near-cloud-top characteristics) can still provide useful physical insights into thunderstorm properties. Thus, the success criteria for this lidar-based analysis were modest, and the primary goals were to demonstrate weak yet statistically significant (and physically meaningful) correlations between lightning and cloud properties.

First, the CATS hydrometeor feature mask was analyzed when lightning was detected by LIS. For this, the analysis took advantage of the fact that the CATS hydrometeor mask uses an increasing index scale ranging from 0 (no cloud), to 1 (liquid cloud), to 2 (undetermined cloud phase), to 3 (ice cloud), and determined the frequency of the highest value index within 50 km of lightning along the CATS ground track. The results are shown in Fig. 3. Over 90% of profiles with lightning were associated with ice-phase or undetermined (likely mixed-phase) cloud. Only ~7% of profiles were associated with liquid cloud. Assuming that CATS is not providing evidence of solely warm-phase clouds producing lightning, this suggests that CATS' hydrometeor mask can identify ice-containing cloud with better than 90% accuracy (notable given validation of radar-based hydrometeor identification is difficult; e.g., Ryzhkov et al., 2005), and thus demonstrates the value of using lightning observations to validate remote sensing of hydrometeor type. Moreover, given that lidar cannot penetrate deeply into optically thick clouds, one cannot rule out the presence of ice below the cloud-top-biased lidar observations, nor can one rule out the fundamental differences in LIS and CATS sampling geometry contributing to any discrepancies. The very small number of "no cloud" observations are also notable and will be analyzed in detail later in the next subsection.

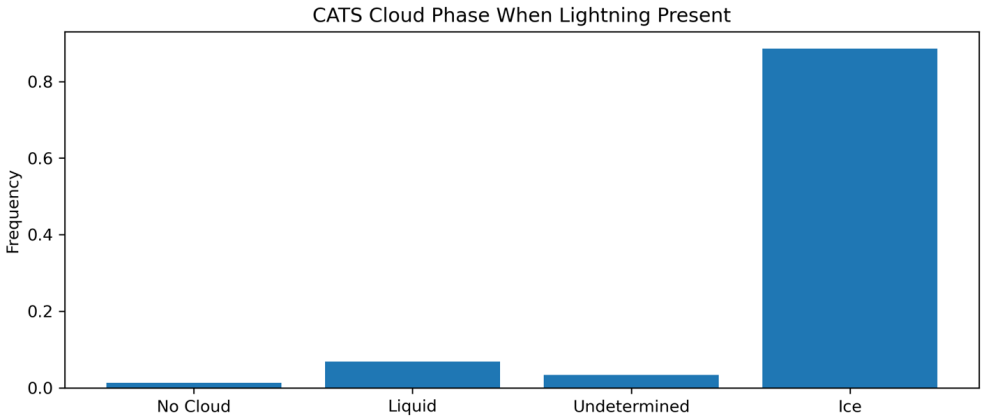

Figure 3. Bar plot showing frequency of "maximum" CATS cloud-top phase index when at least one LIS flash was detected.

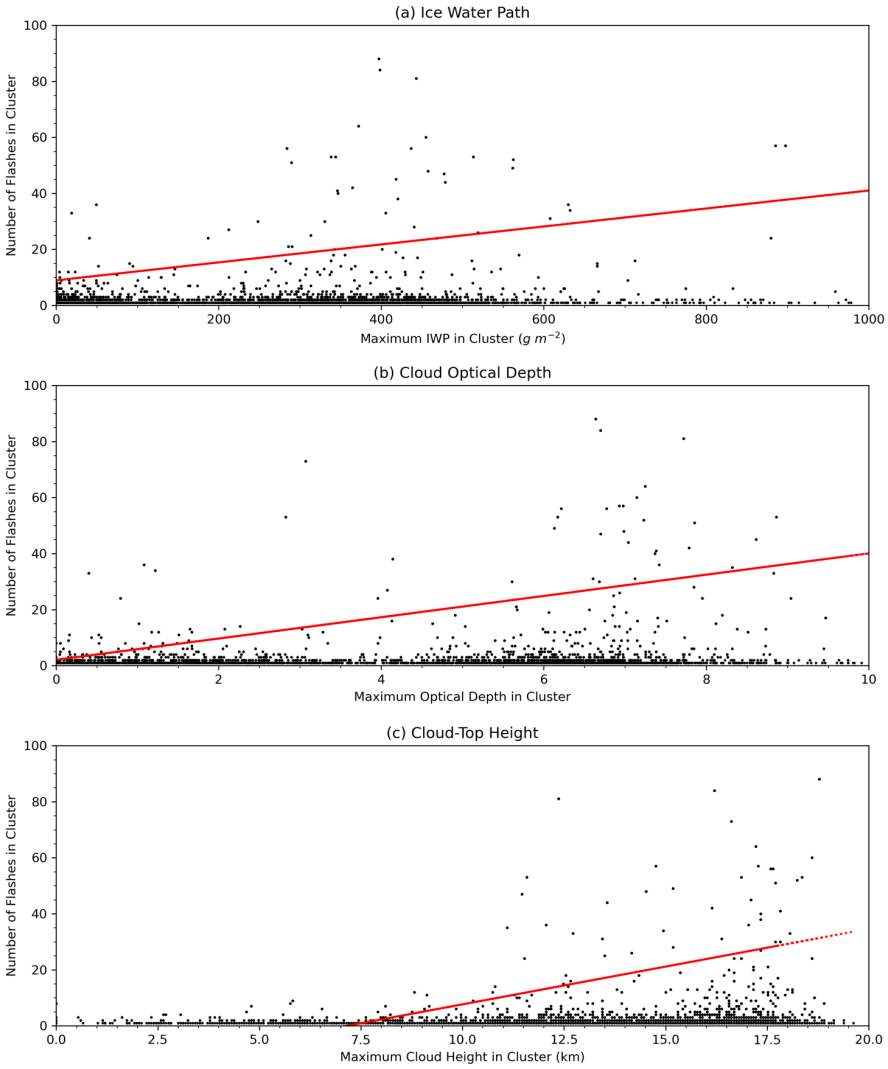

Figure 4. (a) Maximum CATS IWP near a cluster of ISS LIS flashes vs. number of flashes in the cluster. The best-fit line is shown in red. (b) Maximum CATS cloud optical depth near a cluster of ISS LIS flashes vs. number of flashes in the cluster. The best-fit line is shown in red. (c) Maximum CATS cloud-top height near a cluster of ISS LIS flashes vs. number of flashes in the cluster. The best-fit line is shown in red.

Next, LIS-detected flashes were clustered following the methodology described in Section 2.3 and compared to the maximum CATS-inferred cloud properties (IWP, cloud-top height, and optical depth) within 50 km of the cluster along the CATS ground track, and the results are shown in Fig. 4. At first glance, the results are not as good as radar-lightning analyses (e.g., Wiens et al., 2005), but

in all subpanels the best-fit lines have Spearman correlations ranging between +0.38-0.42, with significance values > 99%. That is, the analysis found that linear correlations between a proxy for lightning flash rate and IWP (Fig. 4a), cloud optical depth (Fig. 4b), and cloud-top height (Fig. 4c) were all positive (which is expected and physically meaningful) and highly statistically significant. These metrics demonstrate the utility of comparing lightning measurements with lidar-inferred cloud properties, satisfying the success criteria for this analysis. Higher-power polynomial fitting (e.g., 5th power relationships like Price and Rind, 1992) was not attempted due to the relatively small number of samples available in this study. Instead, the focus was simply to determine whether simple yet statistically significant relationships could be found.

3.3 Using lidar to explore LIS false-alarm rate

Blakeslee et al. (2020) reported an ISS LIS false alarm rate (FAR) under 5%, based on comparisons with other reference lightning datasets. This FAR likely results from unfiltered radiation-induced noise as well as a combination of unfiltered cloud-based and surface-based solar glint. The latter is nominally controlled by a surface glint filter already contained within the ISS LIS processing code. This filter checks for the continuous occurrence of transients over many successive frames (not just intermittently like lightning) in a location that stays fixed within the instrument's frame of reference (similar to how solar glint appears to an observer when viewing from, e.g., an airplane flying over the sunlit ocean). It would be useful to use CATS "no cloud" null cases (Fig. 3) to evaluate the performance of this surface glint filter.

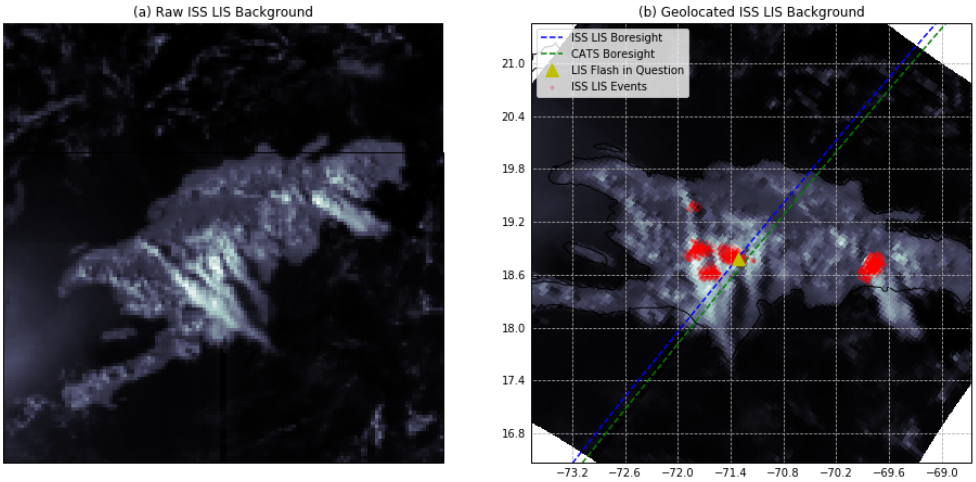

Figure 5. (a) Raw, un-geolocated ISS LIS background image from approxi-

mately 2044 UTC on 1 June 2017. (b) The same ISS LIS background image but geolocated, showing ISS LIS events detected in the domain of the image during the overpass. The suspect LIS flash not seen near CATS-inferred cloud also is indicated, and LIS and CATS boresight ground tracks are shown.

Of the 8246 LIS/CATS matchups, 105 (1.3%) have no CATS-identified cloud within 50 km along the CATS ground track (further constrained by the flash centroid needing to be within 25 km distance perpendicular to the CATS ground track). Of these 105 candidate false alarms, 65 occurred during daytime (777.4 nm backgrounds during night have limited utility for this paper's analysis) and have nearly coincident ISS LIS backgrounds (within approximately 30-60 seconds, the frequency with which LIS provides background imagery, as discussed in Section 2.3).

Manual review of these geolocated backgrounds, with LIS lightning overlaid, was performed. This analysis found that the vast majority of candidate false alarms were similar to Fig. 5, where obvious convection (in this case, over Hispaniola) is in the LIS field of view and the presence of lightning is reasonable to infer. This case demonstrates the fundamental limitations of co,paring 2D horizontal lightning observations with lidar nadir curtains: Sometimes, obvious connections are just missed. Tightening distance thresholds obviously would improve on this, at the cost of reducing the total size of the already small LIS/CATS dataset. At the same time, the fact that only ~1% of LIS/CATS comparisons with the chosen distance thresholds couldn't find at least some cloud in the vicinity of lightning is highly encouraging for the approach adopted in this study.

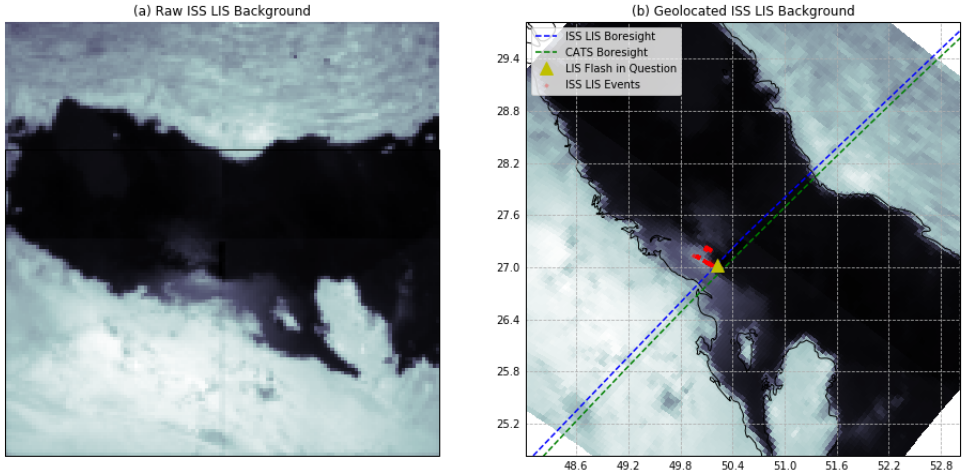

Figure 6. (a) Raw, un-geolocated ISS LIS background image from approximately 0953 UTC on 9 August 2017. (b) The same ISS LIS background image but geolocated, showing ISS LIS events detected in the domain of the image during the overpass. The suspect LIS flash not seen near CATS-inferred cloud also is indicated, and LIS and CATS boresight ground tracks are shown.

Further analysis found only 6 instances where there were no apparent clouds in the LIS backgrounds. An example is shown in Fig. 6, which appears to show glint from a water surface (in this case, the Persian Gulf) made it through LIS data filters. Other cases (not shown) suggest that snow fields in mountainous regions also may have contributed to these false alarms. Overall, this analysis demonstrated that the surface glint-based FAR for ISS LIS is ~0.1% during daytime (6 confirmed false alarms out of 65 candidates, which themselves only represented ~1% of the daytime matchup dataset). Since these surface glint filters were inherited from the long-term TRMM LIS mission, this excellent performance is a highly encouraging sign of the quality of the long-term combined LIS dataset (1997-present).

4. Discussion and Conclusions

This was a pathfinder study that made use of a short (~8-month) overlapping dataset to explore the viability of combining spaceborne lidar and lightning observations to study thunderstorms. The results demonstrate that lidar observations can provide insight into the global thunderstorm climatology, are realistically correlated with lightning characteristics such as flash rate despite the lack of deep penetration into thunderclouds, and enable new methods for quality control and validation of spaceborne optical lightning observations.

Specifically, this study found that lidar-inferred cloud tops near lightning behave realistically given how the tropopause slopes downward from the tropics to the poles. In addition, these cloud-tops average approximately 2-km higher in altitude compared to radar-based climatologies using 20-dBZ echo tops. This demonstrated the advantage of using lidar as a more accurate measure of cloud-top height compared to less-sensitive Ku-band radar (e.g., TRMM, GPM), but at the same time also points toward a way to use lidar to help scale radar-based climatologies to more accurately convert echo-top heights to cloud-top heights.

Moreover, this study found that a proxy for lightning flash rate shows reasonable behavior relative to lidar-retrieved cloud properties, such as cloud optical depth, cloud-top height, and IWP. The results also demonstrated that CATS' cloud-top phase retrieval worked with likely 90% or better accuracy.

Finally, this study determined that the false alarm rate for LIS-identified flashes associated with no nearby cloud (e.g., solar glint off water) is ~0.1%. This demonstrated that the surface glint filters in the ISS LIS processing code (inherited from the much longer TRMM dataset) are working extremely well and that surface glint likely is a nearly negligible contributor to LIS false alarms (which have been estimated at less than 5% of the LIS dataset; Blakeslee et al., 2020). This is in contrast to, e.g., GLM where surface glint has been a major contributor to

false alarms, particularly before implementation of the blooming filter in GLM processing (Rudlosky et al., 2019).

Based on this pathfinder study, fruitful scientific insights are expected from larger combined lidar/lightning datasets. These could include analysis combining GLM with the Cloud-Aerosol Lidar with Orthogonal Polarization (CALIOP; Winker, 2022). In addition to building on the analyses performed in the present study, such an analysis could use CALIOP to help validate stereo retrievals of cloud-top height from dual GLM observations (Mach & Virts, 2021). Moreover, potential future datasets, including a lidar (or lidars) hosted on the AOS mission, are also exploitable using lessons learned from this study. These larger datasets potentially could mitigate some of the limitations of this study, specifically the short time period used here, which didn't even cover one full annual cycle. Moreover, a larger dataset also would enable the use of tighter time/distance thresholds for defining instrument conjunctions, potentially leading to more accurate comparisons.

In addition, a larger number of samples may allow for detailed investigation of aerosol interactions with thunderstorms. Since lidar can determine aerosol type (e.g., Omar et al., 2009), lightning enhancement (or suppression) by smoke, dust, and other aerosol types could be studied.

Acknowledgments

The authors thank members of the NASA Marshall lightning group – including Dan Cecil, Patrick Gatlin, Bill Koshak, Doug Mach, Mason Quick, and Chris Schultz – for helpful discussions regarding this study's results. Rich Blakeslee (NASA Emeritus) served as the original Principal Investigator for ISS LIS. This research and the ISS LIS mission itself are funded by NASA's Earth from ISS program. In particular, the support of ISS LIS by key NASA Headquarters personnel – including Jamie Wicks, Warren Case, Paul Brandinger, Will McCarty, Aaron Piña, Tsengdar Lee, and the late Gail Skofronick-Jackson – is gratefully acknowledged. The authors declare no conflicts of interest.

Open Research

ISS LIS data are available from the Global Hydrometeorology Resource Center (GHRC) Distributed Active Archive Center (DAAC) via the Digital Object Identifiers (DOIs) listed in the Blakeslee (2020a, b) references. The TRMM and GPM RPF data (with LIS and WWLLN) are available for public download from http://atmos.tamucc.edu/trmm/data/. CATS data are hosted on the instrument's archive at https://cats.gsfc.nasa.gov/data/. The ISS_Camera_Geolocate software is available from the Lang (2019) reference. The primary programming language used in the CATS/LIS analysis was Python 3.7, with significant use of the following packages: numpy, scipy, matplotlib, xarray, and h5py. Interactive Data Language (IDL; https://www.l3harrisgeospatial.com/Software-Technology/IDL) was used for

the TRMM/GPM analysis.

References

Allen, D. J., Pickering, K. E., Lamsal, L., Mach, D. M., Quick, M. G., Lapierre, J., et al. (2021). Observations of lightning NOx production from GOES-R post launch test field campaign flights. Journal of Geophysical Research: Atmospheres, 126, e2020JD033769. https://doi.org/10.1029/2020JD033769

AOS, cited 2022. Atmosphere Observing System. [Available online at https://aos.gsfc.nasa.gov/.]

Avery, M., Winker, D., Heymsfield, A., Vaughan, M., Young, S., Hu, Y., and Trepte, C. (2012), Cloud ice water content retrieved from the CALIOP space-based lidar, Geophys. Res. Lett., 39, L05808, doi:10.1029/2011GL050545.

Blakeslee, R.J., Lang, T.J., Koshak, W.J., Buechler, D., Gatlin, P., Mach, D.M., Stano, G.T., Virts, K.S., Walker, T.D., Cecil, D.J., Ellett, W., Goodman, S.J., Harrison, S., Hawkins, D.L., Heumesser, M., Lin, H., Maskey, M., Schultz, C.J., Stewart, M., Bateman, M., Chanrion, O. and Christian, H. (2020), Three Years of the Lightning Imaging Sensor Onboard the International Space Station: Expanded Global Coverage and Enhanced Applications. J. Geophys. Res. Atmos., 125: e2020JD032918. https://doi.org/10.1029/2020JD032918

Blakeslee, Richard J. (2020a). Quality Controlled Lightning Imaging Sensor (LIS) on International Space Station (ISS) Science Data. Dataset available online from the NASA Global Hydrometeorology Resource Center DAAC, Huntsville, Alabama, U.S.A. DOI: http://dx.doi.org/10.5067/LIS/ISSLIS/DATA108

Blakeslee, Richard J. (2020b). Quality Controlled Lightning Imaging Sensor (LIS) on International Space Station (ISS) Backgrounds. Dataset available online from the NASA Global Hydrometeorology Resource Center DAAC, Huntsville, Alabama, U.S.A. DOI: http://dx.doi.org/10.5067/LIS/ISSLIS/DATA208

Campbell, J. R., Sassen, K., McGill, M. J., & Hart, W. D. (2005, January). Lidar depolarization ratios from CRYSTAL-FACE thunderstorm anvils. In Preprints of 2nd Symp. Lidar Atmospheric Monitoring, P (Vol. 1).

Carey, L.D.; Schultz, E.V.; Schultz, C.J.; Deierling, W.; Petersen, W.A.; Bain, A.L.; Pickering, K.E. An Evaluation of Relationships between Radar-Inferred Kinematic and Microphysical Parameters and Lightning Flash Rates in Alabama Storms. Atmosphere 2019, 10, 796. https://doi.org/10.3390/atmos10120796

Ceolato, R., & Berg, M. J. (2021). Aerosol light extinction and backscattering: A review with a lidar perspective. Journal of Quantitative Spectroscopy and Radiative Transfer, 262, 107492.

Cui, Z., Pu, Z., Emmitt, G. D., & Greco, S. (2020). The Impact of Airborne Doppler Aerosol Wind (DAWN) Lidar Wind Profiles on Numerical Simulations

of Tropical Convective Systems during the NASA Convective Processes Experiment (CPEX), Journal of Atmospheric and Oceanic Technology, 37(4), 705-722. https://doi.org/10.1175/JTECH-D-19-0123.1

Delanoë, J., and Hogan, R. J. (2010), Combined CloudSat-CALIPSO-MODIS retrievals of the properties of ice clouds, J. Geophys. Res., 115, D00H29, doi:10.1029/2009JD012346.

Ester, M., H. P. Kriegel, J. Sander, and X. Xu, "A Density-Based Algorithm for Discovering Clusters in Large Spatial Databases with Noise". In: Proceedings of the 2nd International Conference on Knowledge Discovery and Data Mining, Portland, OR, AAAI Press, pp. 226-231. 1996

Hagihara, Y., Okamoto, H., and Luo, Z. J. (2014), Joint analysis of cloud top heights from CloudSat and CALIPSO: New insights into cloud top microphysics, J. Geophys. Res. Atmos., 119, 4087– 4106, doi:10.1002/2013JD020919.

Heymsfield, G. M., & Fulton, R. (1988). Comparison of High-Altitude Remote Aircraft Measurements with the Radar Structure of an Oklahoma Thunderstorm: Implications for Precipitation Estimation from Space, Monthly Weather Review, 116(5), 1157-1174. https://doi.org/10.1175/1520-0493(1988)116<1157:COHARA>2.0.CO;2

Holmlund, K., Grandell, J., Schmetz, J., Stuhlmann, R., Bojkov, B., Munro, R., Lekouara, M., Coppens, D., Viticchie, B., August, T., Theodore, B., Watts, P., Dobber, M., Fowler, G., Bojinski, S., Schmid, A., Salonen, K., Tjemkes, S., Aminou, D., & Blythe, P. (2021). Meteosat Third Generation (MTG): Continuation and Innovation of Observations from Geostationary Orbit, Bulletin of the American Meteorological Society, 102(5), E990-E1015. https://doi.org/10.1175/BAMS-D-19-0304.1

Hou, A. Y., Kakar, R. K., Neeck, S., Azarbarzin, A. A., Kummerow, C. D., Kojima, M., Oki, R., Nakamura, K., & Iguchi, T. (2014). The Global Precipitation Measurement Mission, Bulletin of the American Meteorological Society, 95(5), 701-722.

Khain, A., Rosenfeld, D. and Pokrovsky, A. (2005), Aerosol impact on the dynamics and microphysics of deep convective clouds. Q.J.R. Meteorol. Soc., 131: 2639-2663. https://doi.org/10.1256/qj.04.62

Kumjian, M. R., & Ryzhkov, A. V. (2008). Polarimetric Signatures in Supercell Thunderstorms, Journal of Applied Meteorology and Climatology, 47(7), 1940-1961. https://doi.org/10.1175/2007JAMC1874.1

Kummerow, C., Barnes, W., Kozu, T., Shiue, J., & Simpson, J. (1998). The Tropical Rainfall Measuring Mission (TRMM) Sensor Package, Journal of Atmospheric and Oceanic Technology, 15(3), 809-817.

Lang, T. J. (2019). ISS Camera Geolocate Python module, doi: 10.5281/zenodo.2585824. [Available online at https://github.com/nasa/ISS_Camera_Geolocate]

Liu, C. (2020). GPM Precipitation Feature Database Description, Version 2.0. Texas A&M University at Corpus Christi, Corpus Christi, TX. http://atmos.tamucc.edu/trmm/

Liu, C., and Zipser, E. J. (2005), Global distribution of convection penetrating the tropical tropopause, J. Geophys. Res., 110, D23104, doi:10.1029/2005JD006063.

Liu, C., Zipser, E. J., Cecil, D. J., Nesbitt, S. W., & Sherwood, S. (2008). A Cloud and Precipitation Feature Database from Nine Years of TRMM Observations, Journal of Applied Meteorology and Climatology, 47(10), 2712-2728.

López, R. E., and Aubagnac, J.-P. (1997), The lightning activity of a hailstorm as a function of changes in its microphysical characteristics inferred from polarimetric radar observations, J. Geophys. Res., 102(D14), 16799– 16813, doi:10.1029/97JD00645.

Mace, G. G., Zhang, Q., Vaughan, M., Marchand, R., Stephens, G., Trepte, C., and Winker, D. (2009), A description of hydrometeor layer occurrence statistics derived from the first year of merged Cloudsat and CALIPSO data, J. Geophys. Res., 114, D00A26, doi:10.1029/2007JD009755.

MacGorman, D. R., M. S. Elliott, and E. DiGangi (2017), Electrical discharges in the overshooting tops of thunderstorms, J. Geophys. Res. Atmos., 122, 2929–2957, doi:10.1002/ 2016JD025933.

Mach, D., & Virts, K. (2021). A Technique for Determining Three-Dimensional Storm Cloud-Top Locations Using Stereo Optical Lightning Pulses Observed from Orbit, Journal of Atmospheric and Oceanic Technology, 38(11), 1993-2001. https://doi.org/10.1175/JTECH-D-21-0078.1

Matthew McGill, Dennis Hlavka, William Hart, V. Stanley Scott, James Spinhirne, and Beat Schmid, "Cloud Physics Lidar: instrument description and initial measurement results," Appl. Opt. 41, 3725-3734 (2002)

McGill, M. J., Li, L., Hart, W. D., Heymsfield, G. M., Hlavka, D. L., Racette, P. E., Tian, L., Vaughan, M. A., and Winker, D. M. (2004), Combined lidar-radar remote sensing: Initial results from CRYSTAL-FACE, J. Geophys. Res., 109, D07203, doi:10.1029/2003JD004030.

McGill, M. J., Vaughan, M. A., Trepte, C. R., Hart, W. D., Hlavka, D. L., Winker, D. M., and Kuehn, R. (2007), Airborne validation of spatial properties measured by the CALIPSO lidar, J. Geophys. Res., 112, D20201, doi:10.1029/2007JD008768.

Omar, A. H., Winker, D. M., Vaughan, M. A., Hu, Y., Trepte, C. R., Ferrare, R. A., Lee, K., Hostetler, C. A., Kittaka, C., Rogers, R. R., Kuehn, R. E., & Liu, Z. (2009). The CALIPSO Automated Aerosol Classification and Lidar Ratio Selection Algorithm, Journal of Atmospheric and Oceanic Technology, 26(10), 1994-2014. https://doi.org/10.1175/2009JTECHA1231.1

Price, C., and Rind, D. (1992), A simple lightning parameterization for calculating global lightning distributions, J. Geophys. Res., 97(D9), 9919– 9933, doi:10.1029/92JD00719.

Quick, M. G., Christian, H. J., Virts, K. S., & Blakeslee, R. J. (2020). Airborne radiometric validation of the geostationary lightning mapper using the Fly's Eye GLM Simulator. Journal of Applied Remote Sensing, 14(4), 044518.

Rudlosky, S. D., Goodman, S. J., Virts, K. S., & Bruning, E. C. (2019). Initial geostationary lightning mapper observations. Geophysical Research Letters, 46, 1097– 1104. https://doi.org/10.1029/2018GL081052

Rust, W., Doviak, R. Radar research on thunderstorms and lightning. Nature 297, 461–468 (1982). https://doi.org/10.1038/297461a0

Rutledge, S. A., Hilburn, K. A., Clayton, A., Fuchs, B., & Miller, S. D. (2020). Evaluating Geostationary Lightning Mapper flash rates within intense convective storms. Journal of Geophysical Research: Atmospheres, 125, e2020JD032827. https://doi.org/10.1029/2020JD032827

Ryzhkov, A. V., Schuur, T. J., Burgess, D. W., Heinselman, P. L., Giangrande, S. E., & Zrnic, D. S. (2005). The Joint Polarization Experiment: Polarimetric Rainfall Measurements and Hydrometeor Classification, Bulletin of the American Meteorological Society, 86(6), 809-824. https://doi.org/10.1175/BAMS-86-6-809

Santer, B. D., et al., Behavior of tropopause height and atmospheric temperature in models, reanalyses, and observations: Decadal changes, J. Geophys. Res., 108(D1), 4002, doi:10.1029/2002JD002258, 2003.

Sassen, K. (1977). Lidar Observations of High Plains Thunderstorm Precipitation, Journal of Atmospheric Sciences, 34(9), 1444-1457. https://doi.org/10.1175/1520-0469(1977)034<1444:LOOHPT>2.0.CO;2

Sassen, K., Benson, R. P., & Spinhirne, J. D. (2000). Tropical cirrus cloud properties derived from TOGA/COARE airborne polarization lidar. Geophysical Research Letters, 27(5), 673-676. https://doi.org/10.1029/1999GL010946

Schultz, C. J., Lang, T. J., Leake, S., Runco, M., & Stefanov, W. (2021). A technique for automated detection of lightning in images and video from the International Space Station for scientific understanding and validation. Earth and Space Science, 8, e2020EA001085. https://doi.org/10.1029/2020EA001085

Sherwood, S. C., Chae, J.-H., Minnis, P., and McGill, M. (2004), Underestimation of deep convective cloud tops by thermal imagery, Geophys. Res. Lett., 31, L11102, doi:10.1029/2004GL019699.

Tatsuo Shiina, Toshio Honda, and Tetsuo Fukuchi "Examination of lidar lightning measurement", Proc. SPIE 6409, Lidar Remote Sensing for Environmental Monitoring VII, 64090Y (12 December 2006); https://doi.org/10.1117/12.693735

van Diedenhoven, B., A. M. Fridlind, B. Cairns, A. S. Ackerman, and

J. E. Yorks (2016), Vertical variation of ice particle size in convective cloud tops, Geophys. Res. Lett., 43, 4586–4593, doi:10.1002/2016GL068548.

Virts, K. S., Wallace, J. M., Hutchins, M. L., & Holzworth, R. H. (2013). Highlights of a New Ground-Based, Hourly Global Lightning Climatology, Bulletin of the American Meteorological Society, 94(9), 1381-1391.

Wang, L., Follette-Cook, M. B., Newchurch, M. J., Pickering, K. E., Pour-Biazar, A., Kuang, S., ... & Peterson, H. (2015). Evaluation of lightning-induced tropospheric ozone enhancements observed by ozone lidar and simulated by WRF/Chem. Atmospheric Environment, 115, 185-191.

Wiens, K. C., Rutledge, S. A., & Tessendorf, S. A. (2005). The 29 June 2000 Supercell Observed during STEPS. Part II: Lightning and Charge Structure, Journal of the Atmospheric Sciences, 62(12), 4151-4177. https://doi.org/10.1175/JAS3615.1

Winker, D. M. (2022). The CALIPSO Lidar: Aerosol Observations for Air Quality and Climate. In Handbook of Air Quality and Climate Change (pp. 1-13). Singapore: Springer Singapore.

Dave Winker, Mark Vaughan, Bill Hunt, "The CALIPSO mission and initial results from CALIOP," Proc. SPIE 6409, Lidar Remote Sensing for Environmental Monitoring VII, 640902 (12 December 2006); https://doi.org/10.1117/12.698003

Yorks, J. E., M. J. McGill, S. P. Palm, D. L. Hlavka, P. A. Selmer, E. P. Nowottnick, M. A. Vaughan, S. D. Rodier, and W. D. Hart (2016), An overview of the CATS level 1 processing algorithms and data products, Geophys. Res. Lett., 43, 4632–4639, doi:10.1002/2016GL068006.

Yoshida, R., Okamoto, H., Hagihara, Y., and Ishimoto, H. (2010), Global analysis of cloud phase and ice crystal orientation from Cloud-Aerosol Lidar and Infrared Pathfinder Satellite Observation (CALIPSO) data using attenuated backscattering and depolarization ratio, J. Geophys. Res., 115, D00H32, doi:10.1029/2009JD012334.